Biochimica et Biophysica Acta 1844 (2014) 2290–2297

Contents lists available at ScienceDirect

Biochimica et Biophysica Acta

journal homepage: www.elsevier.com/locate/bbapap

γ-Glutamyl transpeptidase architecture: Effect of extra sequence deletion on autoprocessing, structure and stability of the protein from *Bacillus licheniformis*

Meng-Chun Chi [a], Yi-Hui Lo [a], Yi-Yu Chen [a], Long-Liu Lin [a,*], Antonello Merlino [b,c,*]

[a] Department of Applied Chemistry, National Chiayi University, 300 Syuefu Road, Chiayi City 600, Taiwan
[b] Department of Chemical Sciences, University of Naples Federico II, Napoli, Italy
[c] Istituto di Biostrutture e Bioimmagini, CNR, Napoli, Italy

ARTICLE INFO

Article history:
Received 24 July 2014
Received in revised form 30 August 2014
Accepted 2 September 2014
Available online 10 September 2014

Keywords:
Protein stability
γ-Glutamyl transpeptidase
Ntn hydrolase
Site-directed mutagenesis
Deletion mutants

ABSTRACT

γ-Glutamyl transpeptidases (γ-GTs, EC 2.3.2.2) are a class of ubiquitous enzymes which initiate the cleavage of extracellular glutathione (γ-Glu-Cys-Gly, GSH) into its constituent glutamate, cysteine, and glycine and catalyze the transfer of its γ-glutamyl group to water (hydrolysis), amino acids or small peptides (transpeptidation). These proteins utilize a conserved Thr residue to process their chains into a large and a small subunit that then form the catalytically competent enzyme. Multiple sequence alignments have shown that some bacterial γ-GTs, including that from *Bacillus licheniformis* (*Bl*GT), possess an extra sequence at the C-terminal tail of the large subunit, whose role is unknown. Here, autoprocessing, structure, catalytic activity and stability against both temperature and the chemical denaturant guanidinium hydrochloride of six *Bl*GT extra-sequence deletion mutants have been characterized by SDS-PAGE, circular dichroism, intrinsic fluorescence and homology modeling. Data suggest that the extra sequence has a crucial role in enzyme activation and structural stability. Our results assist in the development of a structure-based interpretation of the autoprocessing reaction of γ-GTs and are helpful to unveil the molecular bases of their structural stability.

1. Introduction

γ-GT catalyzes the transfer of GSH γ-glutamyl group and related γ-glutamyl amides to water (hydrolysis) or to amino acids and peptides (transpeptidation), according to the following scheme [1–4]:

$$\gamma\text{-GluCONHR} + H_2O = Glu + NH_2R \text{ (hydrolysis)}$$

$$\gamma\text{-GluCONHR} + R_1NH_2 = \gamma\text{-GluCONHR}_1 + RNH_2 \text{ (transpeptidation).}$$

In humans, the expression of γ-GT (hGT) is restricted predominantly to the apical surface of ducts and glands where fluids leave the body [5]. The highest concentration of hGT is in the kidney tubules [6], where it prevents excretion of GSH into the urine by cleaving GSH present in the glomerular filtrate. Aberrant expression and localization of hGT are associated with many diseases, including cardiovascular problems [7,8], hypertension [9], diabetes [10] and cancer [11,12]. hGT inhibition is a strategy under development for treatment of various tumors [13]. It has been shown that inhibiting γ-GT prior to chemotherapy or radiation would sensitize γ-GT-positive tumors to treatment [14] and that inhibition of γ-GT activity blocked cisplatin-induced nephrotoxicity in mice [15]. Clinical inhibitors of hGT may be therapeutic also for other diseases, for example for asthma [16].

In bacteria, γ-GTs are found in the cytosol or in the periplasmic space and can be heterodimeric [1,2,17] or heterotetrameric [18,19]. Bacterial γ-GTs have attracted much interest because of their numerous biotechnological applications [1,2,20]; indeed, these proteins can be used as cephalosporin acylases [21] and as glutaminases [22] and can be involved in the enzymatic production of theanine [23], glutamyl phenyl hydrazine analogs [24] and various pharmacological agents [2,20].

Both mammalian and microbial proteins utilize a conserved Thr residue to process its chain into a large and a small subunit that then assemble to form a catalytically competent (generally heterodimeric) enzyme [25–28]. Although it has been shown that precursor protein is more stable than the mature enzyme towards both temperature and chemical denaturation [29,30] and that it can be found in vivo, a physiological role for the precursor is not known.

Multiple sequence alignments have shown that γ-GTs share some features: the catalytic Thr, which is responsible for both the autoprocessing and enzymatic activity, and a Gly-Gly dyad, which is involved in the

* Correspondence to: A. Merlino, Department of Chemical Sciences, University of Naples Federico II, Complesso Universitario di Monte Sant' Angelo, Via Cintia, I-80126 Napoli, Italy. Tel.: +39 081674276; fax: +39 081674090. L.-L. Lin, Department of Applied Chemistry, National Chiayi University, 300 Syuefu Road, Chiayi City 600, Taiwan. Tel: +886 52717969; fax: +886 52717901.
E-mail addresses: llin@mail.ncyu.edu.tw (L.-L. Lin), antonello.merlino@unina.it (A. Merlino).

http://dx.doi.org/10.1016/j.bbapap.2014.09.001
1570-9639/

stabilization of the intermediate that forms during the catalytic process (Fig. S1, A and B) [1,27,28]. On the other hand, some relevant differences have been also underlined. Mammalian γ-GTs are extensively glycosylated [31–33], whereas many microbial γ-GTs lack the lid loop [18,19,34], the region which extends over the active site, and possess an extra sequence at the C-terminal tail of the large subunit [35,36] (Fig. 1A).

Here we have investigated the way in which the protein from *Bacillus licheniformis* (*Bl*GT) responds to change in the length of the extra sequence. The autoprocessing, structure, stability and catalytic activity of six *Bl*GT deletion mutants (Fig. 1B) have been studied.

2. Materials and methods

2.1. Site-directed mutagenesis and protein analyses

A previously constructed plasmid pQE-*Bl*GGT [35], which contains a 1.758-kb insert of *B. licheniformis* genomic DNA with the entire *Bl*GT gene, was used as a template for site-directed mutagenesis. Two overlapping complementary primers with the desired nucleotide changes were designed for each deletion (Table S1). Six deletion mutants (ΔY385–I387, ΔY385–V388, ΔY385–P391, ΔY385–K394, ΔY385–I396 and ΔY385–E398) were constructed by a QuikChange II site-directed mutagenesis kit (Stratagene) according to the manufacturer's instructions. Clones of the recombinant plasmids that had the desired mutations were identified by DNA sequencing with the dideoxynucleotide chain termination method.

*Bl*GT and mutant enzymes were over-expressed in recombinant *Escherichia coli* M15 cells as described previously [36]. Proteins were purified by affinity chromatography with a Ni^{2+}-NTA agarose column under native conditions. The eluted fractions (total volume for each preparation = ~5 mL) were pooled and dialyzed overnight against 500 mL of 50 mM Tris–HCl buffer (pH 8.0) through a 10-kDa cutoff membrane to remove salts. Protein purity was assessed by Coomassie Blue staining of SDS–polyacrylamide gels. Protein concentrations were determined by the Bio-Rad protein assay reagent using bovine serum albumin as a standard.

2.2. Autoprocessing of the enzymes

Autocatalytic processing studies on *Bl*GT and deletion mutants (1 mg mL^{-1}) were performed by incubating the proteins in 50 mM Tris–HCl buffer (pH 8.0) at 4 °C up to 56 days. Aliquots were denatured by boiling in SDS loading buffer for 5 min. Samples were analyzed by SDS-PAGE 12%; the gel was stained using Coomassie Brilliant Blue R-250. The degree of autocatalytic processing was evaluated by measuring the intensity of the protein bands in the gels with a computerized densitometer using CP ATCAS 2.0 program (http://www.lazarsoftware.com).

2.3. Enzyme activity assay and determination of kinetic parameters

The enzyme activity of *Bl*GT and its deletion mutants towards substrate analog L-γ-glutamyl-*p*-nitroanilide (G*p*NA) was determined by measuring the amount of *p*-nitroaniline (*p*NA) released from G*p*NA using the method assay by Tate and Meister (1974) [37]. Briefly, the concentration of *p*NA was measured spectrophotometrically

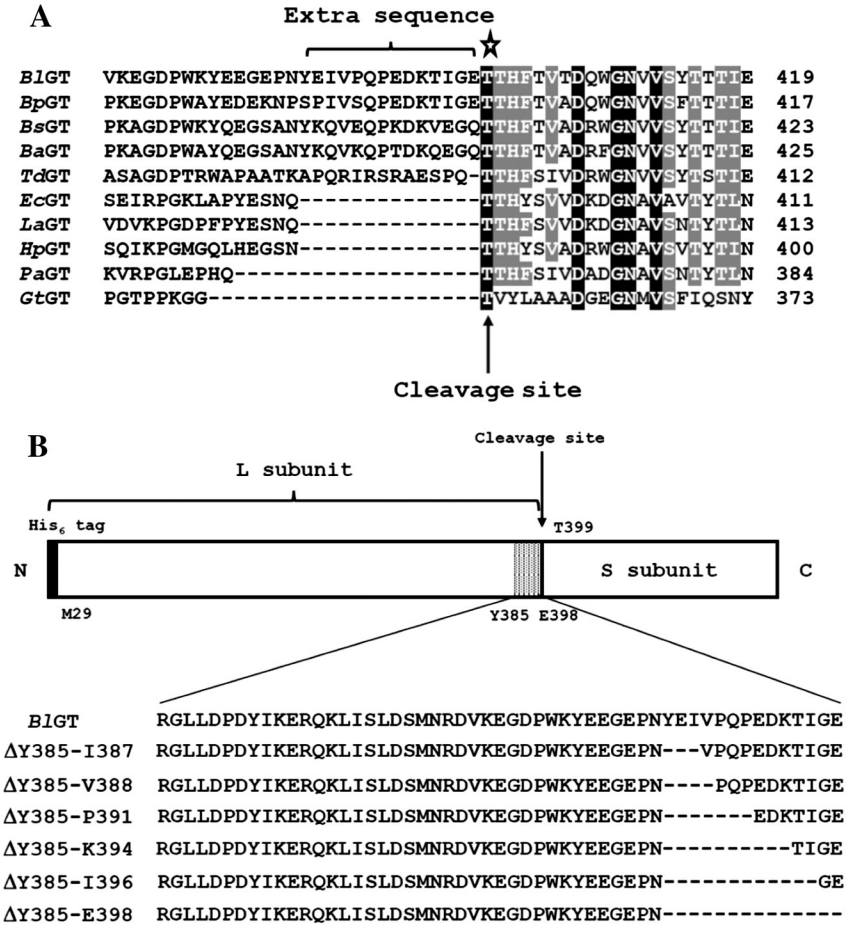

Fig. 1. (A) Multiple sequence alignment of bacterial γ-GTs. The amino acid sequence of *Bl*GT was aligned with those of *B. pumilus*, *B. subtilis*, *B. amyloliquefaciens*, *Thiobacillus denitrificans*, *E. coli*, *Labrenzia aggregate*, *Helicobacter pylori*, *Pseudomonas aeruginosa*, and *Geobacillus thermodenitrificans*. The conserved catalytic Thr responsible for autoprocessing of the enzyme is marked with a star and the extra sequence evidenced. (B) Particular of the sequence of the *Bl*GT deletion mutants that have been analyzed here.

following the adsorption spectrum at 412 nm. Catalytic activity was also measured at different temperatures and as a function of pH, using the following buffers: 50 mM acetate–HCl buffer (pH 3–6), 50 mM Tris–HCl buffer (pH 7–9) and 50 mM glycine–NaOH buffer (pH 10–12).

To evaluate kinetic constants, dependence of the reaction on the substrate concentration was evaluated using fixed amounts of purified *Bl*GT (or of its deletion mutants) incubated with increasing concentrations of G*p*NA from 1 to 1000 μM. Values of K_M and k_{cat} were determined from the non-linear least squares fit of the initial velocity data to the Michaelis–Menten equation.

2.4. Circular dichroism (CD) studies

Far-UV CD spectra of the protein (0.2 mg mL^{-1}) in 50 mM Tris–HCl buffer, pH 8.0, were measured at 25 °C using a JASCO J-815 spectropolarimeter equipped with a Peltier block arrangement (PTC-423S/15), a quartz cuvette of 1 cm path length, and a spectral band pass of 4 nm. Raw ellipticity data were converted to mean residue ellipticity using the formula $[\theta] = [\theta_{raw} \times 100 \times MRW] / c \times l$, where MRW is the mean residue weight for *Bl*GT, c is the concentration of *Bl*GT in mg mL^{-1} and l is the path length in cm. Thermal unfolding curves were registered by monitoring the changes in mean residue ellipticity (at 222 nm) as a function of temperature, for *Bl*GT and its deletion mutants, using a scan rate of 2 °C/min. Deconvolution of CD spectra for secondary structure amount has been performed using CDNN software [38].

2.5. Fluorescence spectroscopy

The fluorescence emission spectra for *Bl*GT and its deletion mutants were recorded at 25 °C using a Jasco FP-6500 spectrophotometer. Spectra were registered between 310 and 450 nm, using a protein concentration of 0.05 mg mL^{-1} in 50 mM Tris–HCl buffer (pH 8.0), upon excitation using $\lambda_{exc} = 280$ nm or $\lambda_{exc} = 295$ nm. The chemical unfolding was evaluated by measuring the emission upon mixing 1 mL guanidinium hydrochloride (GdnHCl) (from 1 to 6 M) with 1 mL of protein (0.05 mg mL^{-1}). Fluorescence was recorded at 25 °C with protein concentration of 0.05 mg mL^{-1} and a final concentration of 0.5–3.0 M GdnHCl in 50 mM Tris–HCl buffer (pH 8.0) using 1 cm quartz cell. The two-state unfolding model (Eq. (1)) was used to calculate the thermodynamic parameters [39].

$$y_{obs} = \frac{\left(y_N + m_f[D]\right) + \left(y_U + m_u[D]\right) \cdot \exp\left[-\left(\Delta G^{H_2O}_{N-U} - m[D]\right)/RT\right]}{1 + \exp\left[-\left(\Delta G^{H_2O}_{N-U} - m[D]\right)/RT\right]}. \quad (1)$$

Then, $[GdnHCl]_{0.5,N-U}$ can be determined from the equation below:

$$[GdnHCl]_{0.5,N-U} = \frac{\Delta G^{H_2O}_{N-U}}{m} \quad (2)$$

where y_{obs} represents the observed biophysical signal, y_N and y_U represent the intercepts, m_f and m_u represent the slopes of the pre- and post-transition baselines, T is the temperature, R is the universal gas constant, $[D]$ is the concentration of GdnHCl, $\Delta G^{H_2O}_{N-U}$ represents the free energy change for the unfolding process, and m is a measure of the dependence of ΔG on GdnHCl concentration.

2.6. Molecular modeling

The models of the precursor and mature forms of the *Bl*GT deletion mutants were obtained using the structures of the T393A variant of *E. coli* γ-GT [26] and of the mature form of *Bl*GT [40] as starting models and the SWISS-MODEL server (http://swissmodel.expasy.org/). The program DeepView-Swiss-PdbViewer [41] was used to build the assembly of the heterodimeric mature enzymes, which was assumed to be similar to that of mature *Bl*GT, to minimize the energy of the structures and calculate the root mean square deviations. The figures have been done with Pymol [42].

3. Results and discussion

3.1. Autoprocessing and structure of *Bl*GT variants

The γ-GTs structurally characterized until now share the same folding pattern. Their overall structure mainly consists of four layers of α-helices and β-sheets (αββα motif) assembled in a kidney shape (Fig. 2). The main structural differences between the diverse γ-GTs are located on the large subunit, on surface loops and at the subunit terminal ends. An interesting feature of some bacterial γ-GTs is the presence of an extra sequence on the C-terminal tail of the large subunit (residues Y385–E398 in the protein from *B. licheniformis*) (Fig. S1). The X-ray structure of *Bl*GT, recently solved [40], suggests that in this enzyme the extra sequence could play an important role in both autoprocessing and enzymatic activity. In particular, the different flexibility of this region in the presence of the substrate highlighted by the comparison between the structure of ligand-free protein and that of its complex with L-Glu has suggested that this region could play a key role in catalysis [40].

In order to verify these hypotheses, autoprocessing, structure, stability and catalytic activity of six new *Bl*GT deletion mutants (ΔY385–I387, ΔY385–V388, ΔY385–P391, ΔY385–K394, ΔY385–I396, and ΔY385–E398) have been investigated. The monitoring of the autocatalytic processing of these *Bl*GT variants has been carried out by incubating the proteins at 4 °C in 50 mM Tris–HCl buffer (pH 8.0) for about 2 months. Aliquots of the deletion mutants have been withdrawn six times in the first two weeks and then once a week up to 56 days and analyzed by SDS-PAGE (Fig. 3A). With the notable exception of ΔY385–E398, which mainly remains as precursor protein even after two months, all the variants are able to autoprocess themselves, leading to the formation of a small and a large subunit with masses of about 41 kDa and 22 kDa, respectively, in about two weeks. However, the ΔY385–P391,

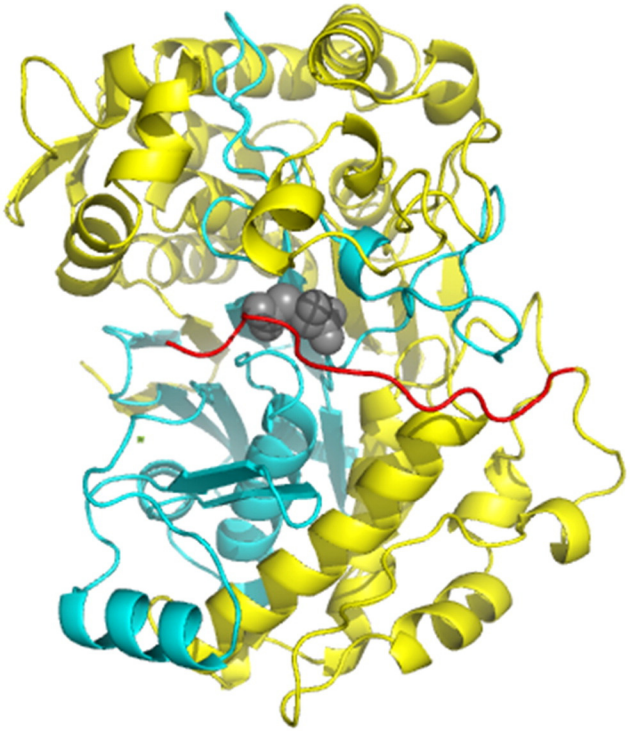

Fig. 2. Ribbon diagram of the structure of *Bl*GT in complex with L-Glu [40]. L-Glu atoms are shown as gray spheres. Small and large subunits are colored in yellow and cyan, respectively. Extra sequence is colored in red.

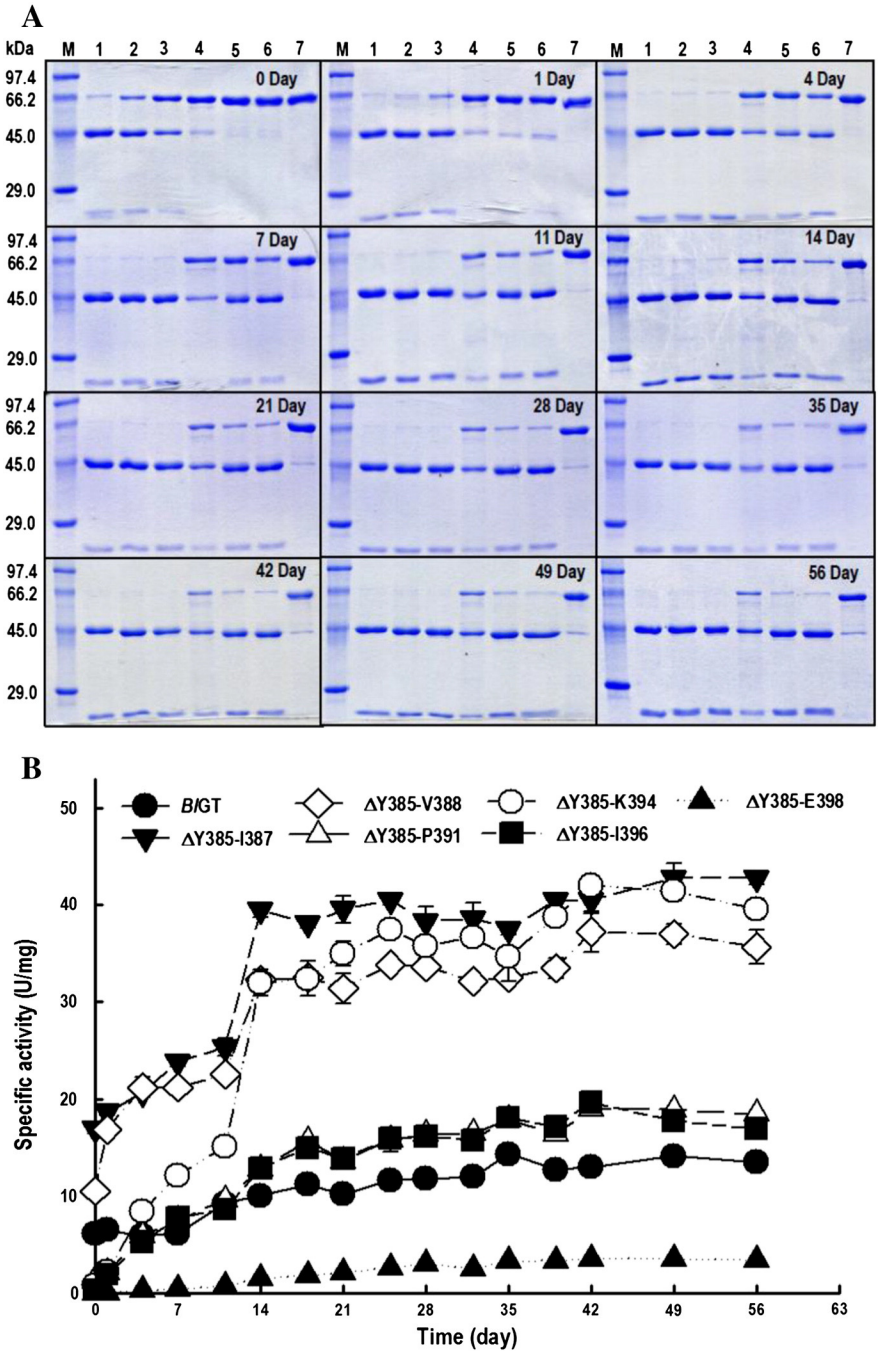

Fig. 3. Autoprocessing and formation of active heterodimeric mature form of *Bl*GT and its deletion mutants evidenced by Coomassie stained SDS-PAGE (A) and following the specific activities (B) as a function of time. In the SDS-PAGE, the following legend has been used: 1. *Bl*GT; 2. ΔY385–I387; 3. ΔY385–V388; 4. ΔY385–P391; 5. ΔY385–K394; 6. ΔY385–I396; 7. ΔY385–E398. Specific activity was determined by monitoring catalysis of *Gp*NA. Each point represents the mean of at least three independent measurements. Error bars represent one standard deviation of uncertainty, calculated on the basis of three experimental measurements.

ΔY385–K394, ΔY385–I396 mutants process themselves more slowly than the other variants. This indicates that the deletion of residues 389–391 (Pro89, Gln390 and Pro391) somewhat affects the enzyme autoprocessing, whereas the whole extra sequence is needed for its proper maturation. In this respect, it should be interesting to note that Gln390 and Pro391 are conserved in *Bl*GT, *Bp*GT, *Bs*GT and *Ba*GT, which are the only γ-GTs with an extra sequence constituted of fourteen residues (Fig. 1A). To study the autoprocessing of the *Bl*GT deletion mutants in more detail, the percentage of processing has been evaluated for each sample, as reported in the Materials and methods section, and plotted as a function of time (Fig. S2). Similar results have been obtained following the time evolution of the specific activity (Fig. 3B). In this case, it is interesting to note the unusual behavior of the Y385–I387 mutant which shows a dramatic increase in the activity between 7 and 14 days, when it is almost completely processed (Fig. S2).

Nevertheless, altogether these data further support the idea that deletion of residues Y385–E398 significantly affects the autoprocessing of the protein.

Since the differences in the rate of autoprocessing observed for the *Bl*GT variants could be linked to conformational variations induced by the deletion, the structure of the six variants has been monitored by analyzing far-UV CD (Fig. 4A) and fluorescence spectra (Fig. 4B) collected at 25 °C. CD spectra of the deletion mutants are almost superimposable to that of *Bl*GT, indicating that the deletions have no significant effect on

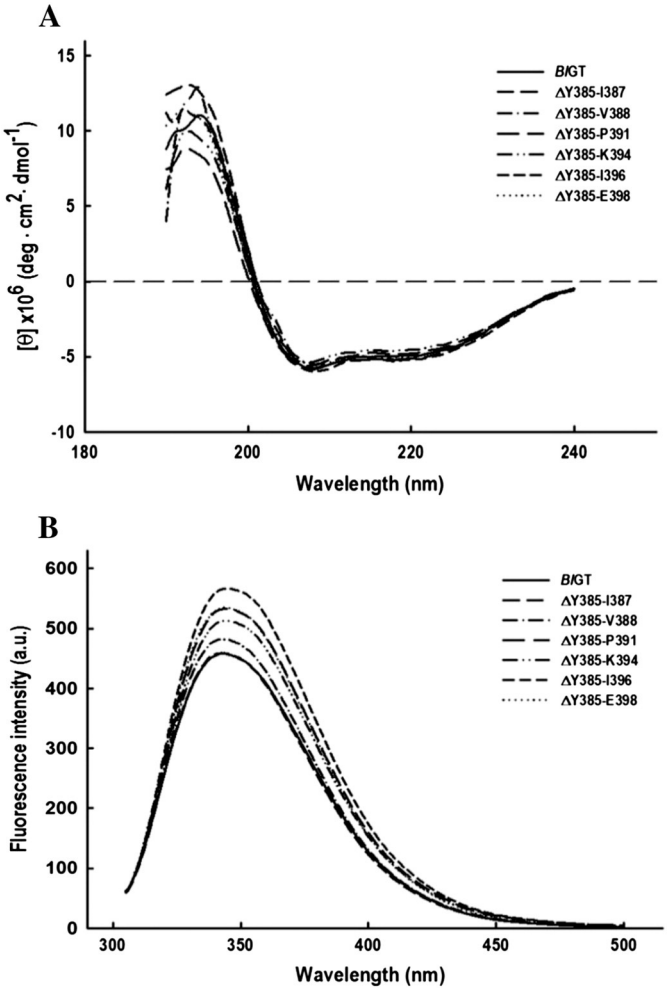

Fig. 4. (A) Far-UV CD spectra of *Bl*GT and its deletion mutants (concentration 0.2 mg mL^{-1}) in 50 mM Trsi–HCl buffer, pH 8.0, recorded at 25 °C. The proteins exhibit a typical α-helical CD profile with minimal peaks at 208 nm and 222 nm. (B) Intrinsic fluorescence spectra of *Bl*GT and its deletion mutants (concentration 0.05 mg mL^{-1}) in 50 mM Tris–HCl buffer, pH 8.0, recorded at 25 °C. Emission fluorescence λ_{max} for ΔY385–I387, ΔY385–V388, ΔY385–P391, ΔY385–K394, ΔY385–I396, and ΔY385–E398 is reported in Table S3. Spectra have been registered using an excitation wavelength of 280 nm.

the secondary structure of the protein. Deconvolution of the spectra reveals that the variants have similar secondary structure content, i.e. 35–40% of alpha helices and 15–20% of beta strands, in close agreement with the X-ray structure of *Bl*GT [40] (Table S2). The comparison of intrinsic fluorescence spectra of the deletion variants reveals that there are just minor shifts in λ_{max} (Table S3), indicating that Trp residues are similarly exposed to the solvent in *Bl*GT and its deletion mutants.

Overall these data suggest that the deletions do not elicit major structural changes on the overall structure of *Bl*GT. To further investigate the consequences of the extra sequence cuttings on the structure of *Bl*GT, the three-dimensional models of both precursor and mature form of the six protein variants have been built, using the X-ray structures of the precursor-like T393A variant of *E. coli* γ-GT [26] and of the mature form of *Bl*GT [40] as templates (Fig. S3). As expected, the overall structures of precursors are very similar to each other (Cα root mean square deviations calculated between the model of ΔY385–I387 and the other five models are in the range 0.44–0.51 Å). The main structural differences are located in the loop regions and in the deletion sites, which adopt different conformations in the various mutants (Fig. S3A). Similarly, the structures of the mature form present significant variations in the deletion regions (Fig. S3B). In this case, the comparison between the structures suggests that the deletion of residues Y385–P391, Y385–K394 and Y385–I396 significantly increases the accessibility of the active site region (Fig. S3C). These findings could well explain the catalytic changes observed for these mutants (see below). More fine perturbations of the structure and dynamics of the protein must be invoked to explain the significant changes in the catalytic activity observed for the ΔY385–I387 and ΔY385–V388 mutants (see below).

3.2. Catalytic activity and structural stability of *Bl*GT deletion mutants

Specific activities of the *Bl*GT variants towards the synthetic substrate G*p*NA have been also studied in comparison to that of *Bl*GT. The results of these experiments are reported in Table 1. All deletion variants exhibit a specific activity significantly altered when compared to *Bl*GT. ΔY385–E398 is inactive, but this is not surprising since it mainly exists as an unprocessed inactive enzyme. ΔY385–P391, ΔY385–K394 and ΔY385–I396 are slightly less active than *Bl*GT, whereas ΔY385–I387 and ΔY385–V388 are the most active variants and are even more active than the wild-type protein. These findings suggest that the deletions introduce minor structural or dynamic changes that affect the catalysis. The relative activity of the deletion mutants has been also characterized as a function of pH and of temperature (Fig. 5A and B, respectively). All the mutants, like *Bl*GT, present their maximum activity at pH 9.0. Optimum temperature of the mutants is between 60 and 72 °C.

The conformational stability of the deletion variants against both temperature and presence of guanidinium hydrochloride (GdnHCl) has been also analyzed by collecting CD spectra as a function of temperature (Fig. 6A) and fluorescence spectra at increasing concentration of GdnHCl (Fig. 6B), respectively. Apparent melting temperature (T_m) and the values of denaturant concentration at half-completion of the transition characterizing the chemical-induced denaturation ($C_{1/2}$) of each analyzed system have been reported in Tables 2 and 3, respectively.

As it clearly emerges from Fig. 6A which shows the temperature-dependence of loss of secondary structure content in *Bl*GT and its mutants, the protein deletion mutants show unfolding curves with different midpoints (T_m values). In particular, the T_m is between 45.3 and 47.9 °C for ΔY385–P391, ΔY385–K394, ΔY385–I396 and ΔY385–E398 whereas it is >60 °C for ΔY385–I387 and ΔY385–V388 and *Bl*GT. Evidently the deletion of the Pro389, Gln390, and Pro391 has resulted in a significant lowering of *Bl*GT apparent melting temperature. These results are in line with those collected measuring the relative activity of the protein as a function of temperature (Fig. S4). The results obtained by denaturation experiments carried out in the presence of GdnHCl are only partly in line with those found denaturing the proteins by

Table 1
Specific activity and kinetic parameters of the purified *Bl*GT and deletion mutant enzymes[a].

Enzyme	K_M (mM)	k_{cat} (s^{-1})	k_{cat}/K_M (mM^{-1} s^{-1})
*Bl*GT	0.37 ± 0.06[b]	12.45 ± 1.23[b]	27.22[b]
ΔY385–I387	0.81 ± 0.07	55.11 ± 2.74	67.92
ΔY385–V388	0.57 ± 0.04	24.41 ± 1.46	43.03
ΔY385–P391	0.76 ± 0.05	4.74 ± 0.41	6.2
ΔY385–K394	0.74 ± 0.05	3.01 ± 0.28	4.09
ΔY385–I396	1.06 ± 0.06	2.09 ± 0.27	1.97
ΔY385–E398	–	–	–

[a] The kinetic parameters were determined for *Bl*GT and the deletion mutants exactly in the same experimental conditions and maturation process time. The parameters were determined from the initial reaction rates at 25 °C and at pH 8.0, in the presence of 1–1000 μM G*p*NA, as previously described. K_M and k_{cat} are the averages of three determinations ± standard deviations.

[b] We have recalculated the values of K_M and k_{cat} also for *Bl*GT in order to perform a more meaningful comparison with the deletion mutants. These values do not match completely, but they are in general agreement, with those that we have previously reported [40]. The small differences in the parameters are probably due to small differences in the maturation process of different batch of *Bl*GT preparations.

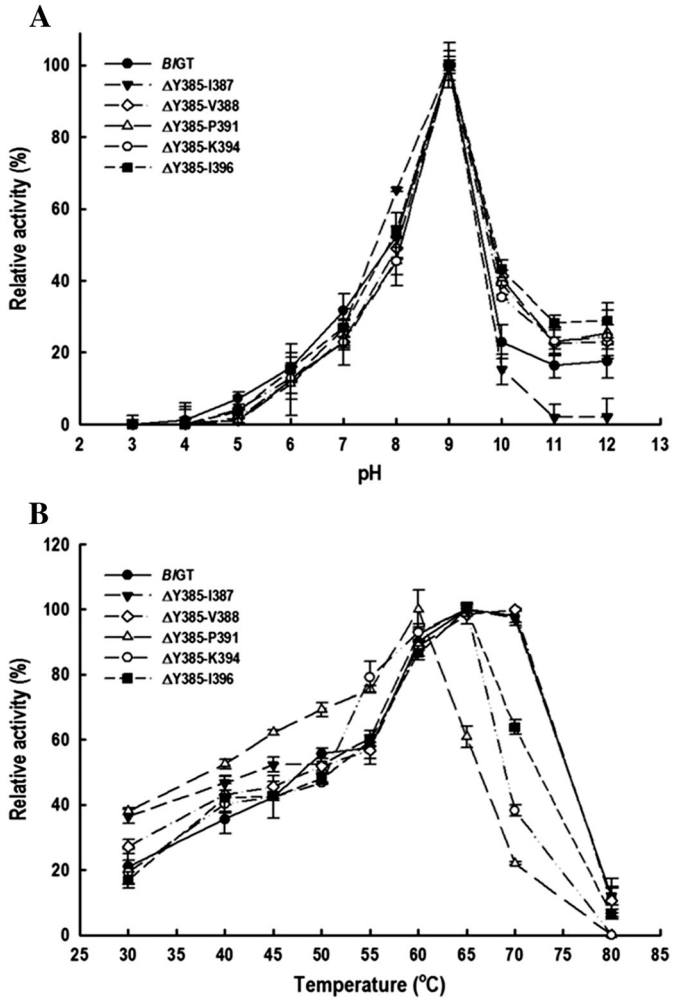

Fig. 5. (A) Relative activity of *Bl*GT and its deletion mutants evaluated as a function of pH (A) and temperature (B). The activity was expressed as a percentage of the highest activity measured over the pH and temperature range examined. Each point represents the mean of at least three independent measurements. Error bars represent one standard deviation of uncertainty.

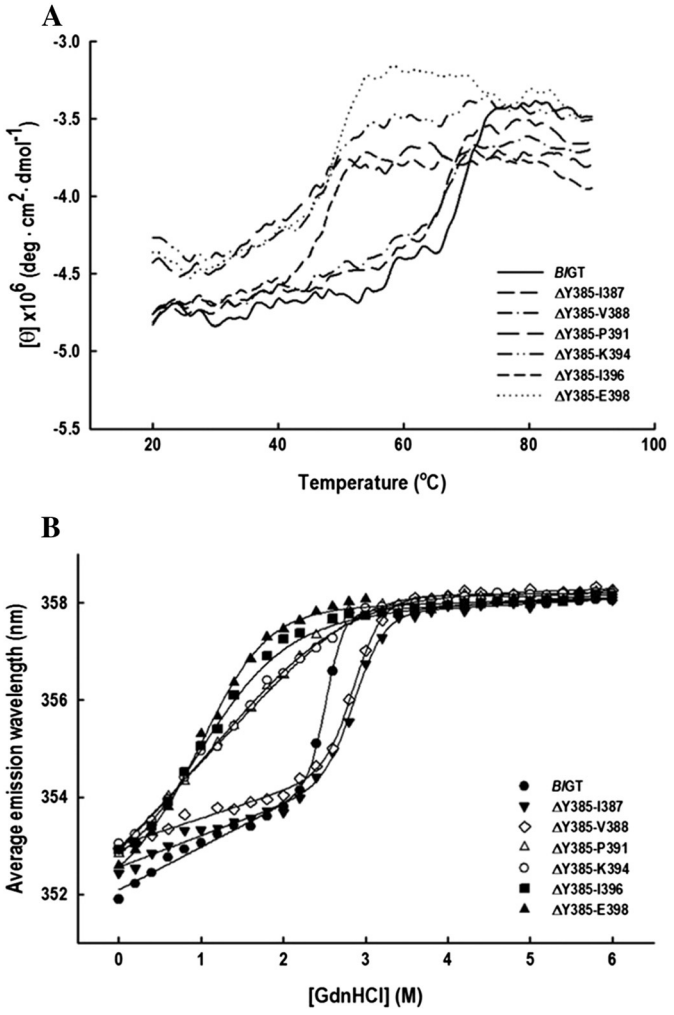

Fig. 6. (A) Thermal unfolding of *Bl*GT and its mutants as followed by CD spectroscopy at 222 nm. (B) GdnHCl-induced denaturation of *Bl*GT and its mutants as followed by monitoring the average emission wavelength at increasing concentrations of guanidine hydrochloride.

thermal unfolding: *Bl*GT, ΔY385–I387, ΔY385–V388 and ΔY385–P391 show a $C_{1/2}$ between 2.6 and 2.9 M, whereas the ΔY385–K394, ΔY385–I396 and ΔY385–E398 variants unfold at 2.0 M, 1.0 M and 1.1 M, respectively (Fig. 6B). Such results suggest that the chemical denaturation of *Bl*GT deletion mutants follows a mechanism different from that used by thermal unfolding, as observed in other protein systems (see for example [43–45]), including members of γ-GT superfamily [29,30]. In the present case, deletion of Pro389, Gln390, and Pro391 does not significantly alter the protein stability against the denaturant, whereas the removal of residues 392–398 has an important role in this process. In this respect, it is interesting to note that this protein region contains three charged residues (Glu392, Asp396, and Lys397) which probably contribute to the chemical stability of *Bl*GT against GdnHCl, in agreement with the well-accepted idea that charged residues play a role in the protein stability against GdnHCl [45,46].

4. Conclusions

Despite the extensive interest in the study of γ-GTs, there is a limited knowledge on the role of specific regions of their sequence on the structure and stability of these proteins. In particular, there is still no paper characterizing the role of the extra sequence on the maturation process of bacterial γ-GTs. Here, we have reported the results of cutting experiments of the extra sequence of the protein from the bacterium *B. licheniformis*. Data reveal that deletion of residues Y385–E398 leaves the protein folding unaffected, but hampers the precursor to process itself in the large and small subunits. Deletion of Y385–I387 results in a large increase in the specific activity of *Bl*GT. Removal of Pro389, Gln390, and Pro391 results in a significant lowering of *Bl*GT apparent melting temperature, whereas removal of chain segment constituted by residues 392–398, where three charge residues are located (Glu392, Asp396, and Lys397), significantly alters the structural stability

Table 2
Summary of the thermal stability of *Bl*GT and its deletion mutants.

Enzyme	T_m (°C)	ΔH_m (kcal mol^{-1})	ΔS_m (cal mol^{-1} K^{-1})	ΔG (25 °C) (kcal mol^{-1} K^{-1})
*Bl*GT	64.7 ± 0.5[a]	79.8 ± 12.6	236.1 ± 3.0	3.7
ΔY385–I387	63.6 ± 1.0	54.0 ± 11.9	160.4 ± 3.9	2.7
ΔY385–V388	61.8 ± 2.3	37.5 ± 12.1	111.9 ± 5.8	2.1
ΔY385–P391	45.3 ± 0.7	62.3 ± 13.4	195.9 ± 4.5	1.4
ΔY385–K394	47.0 ± 1.0	63.2 ± 19.8	197.4 ± 9.6	1.4
ΔY385–I396	46.8 ± 0.6	107.9 ± 29.4	337.3 ± 12.5	3.5
ΔY385–E398	47.9 ± 0.6	97.2 ± 25.9	302.9 ± 10.8	2.2

[a] We have re-measured the thermal stability of *Bl*GT in order to perform a more meaningful comparison with the deletion mutants. The experiments have been performed exactly in the same conditions for *Bl*GT and the deletion mutants (0.2 mg mL^{-1} protein in 50 mM Tris–HCl buffer, pH 8.0).

Table 3
Values of denaturant concentration at half-completion of the transition ($C_{1/2}$) characterizing the chemical-induced denaturation of *Bl*GT and its mutants.

Enzyme	$[GdnHCl]_{0.5,N-U}$ (M)
*Bl*GT	2.6 ± 0.2[a]
ΔY385–I387	2.9 ± 0.1
ΔY385–V388	2.9 ± 0.1
ΔY385–P391	2.6 ± 0.1
ΔY385–K394	2.0 ± 0.1
ΔY385–I396	2.0 ± 0.1
ΔY385–E398	1.1 ± 0.1

[a] We have re-measured the chemical stability of *Bl*GT in order to perform a more meaningful comparison with the deletion mutants. The experiments have been performed exactly in the same conditions for *Bl*GT and the deletion mutants (protein concentration of 0.05 mg mL^{-1} in 50 mM Tris–HCl buffer (pH 8.0)).

of *Bl*GT towards guanidinium hydrochloride. Results also suggest that Gln390 and Pro391 play a role in the protein autoprocessing. Since understanding of the factors responsible for γ-GT folding and stability is important for the production of recombinant enzymes on industrial scale, the knowledge accumulated on the *Bl*GT system could have general implications of great biotechnological significance.

Conflict of interest

The authors declare that they have no conflict of interest.

Acknowledgements

This work was supported by a research grant (NSC-100-2313-B-415-003-MY3) from the National Science Council of Taiwan.

Appendix A. Supplementary data

Supplementary data to this article can be found online at http://dx.doi.org/10.1016/j.bbapap.2014.09.001.

References

[1] I. Castellano, A. Merlino, γ-Glutamyltranspeptidases: sequence, structure, biochemical properties, and biotechnological applications, Cell. Mol. Life Sci. 69 (2012) 3381–3394.
[2] I. Castellano, A. Merlino, γ-Glutamyltranspeptidases. Structure and function, Springer Briefs in Biochemistry and Molecular Biology, VII2013. 1–57 (ISBN: 978-3-0348-0681-7).
[3] J.W. Keillor, A. Menard, R. Castonguay, et al., γ-Glutamyl transpeptidase substrate specificity and catalytic mechanism, J. Phys. Org. Chem. 17 (2004) 529–536.
[4] J.W. Keillor, R. Castonguay, C. Lherbet, Pre-steady-state kinetics studies of rat kidney γ-glutamyl transpeptidase confirm its ping-pong mechanism, Methods Enzymol. 401 (2005) 449–467.
[5] N. Taniguchi, Y. Ikeda, γ-Glutamyl transpeptidase: catalytic mechanism and gene expression, Adv. Enzymol. Relat. Areas Mol. Biol. 72 (1998) 239–278.
[6] A. Meister, S.S. Tate, O.W. Griffith, γ-Glutamyl transpeptidase from kidney, Methods Enzymol. 77 (1981) 237–253.
[7] M. Emdin, C. Passino, A. Pompella, et al., γ-Glutamyltransferase as a cardiovascular risk factor, Eur. Heart J. 27 (2006) 2145–2146.
[8] M. Emdin, C. Passino, M. Franzini, et al., γ-Glutamyl transferase and pathogenesis of cardiovascular disease, Futur. Cardiol. 3 (2007) 263–270.
[9] D.H. Lee, D.R. Jacobs Jr., M. Gross, et al., γ-Glutamyltransferase is a predictor of incident diabetes and hypertension: the coronary artery risk development in young adults (CARDIA) study, Clin. Chem. 49 (2003) 1358–1366.
[10] D.H. Lee, M.H. Ha, J.H. Kim, et al., γ-Glutamyltransferase and diabetes—a 4 year follow-up study, Diabetologia 46 (2003) 359–364.
[11] M.H. Hanigan, γ-Glutamyl transpeptidase, a glutathionase: its expression and function in carcinogenesis, Chem. Biol. Interact. 111-112 (1998) 333–342.
[12] A. Corti, M. Franzini, A. Paolicchi, et al., γ-Glutamyltransferase of cancer cells at the crossroads of tumor progression, drug resistance and drug targeting, Anticancer Res. 30 (2010) 1169–1181.
[13] S. Wickham, N. Regan, M.B. West, J. Thai, P.F. Cook, S.S. Terzyan, P.K. Li, M.H. Hanigan, Inhibition of human γ-glutamyl transpeptidase: development of more potent, physiologically relevant, uncompetitive inhibitors, Biochem. J. 450 (2013) 547–557.
[14] J.B. King, M.B. West, P.F. Cook, M.H. Hanigan, A novel, species-specific class of uncompetitive inhibitors of γ-glutamyl transpeptidase, J. Biol. Chem. 284 (2009) 9059–9065.
[15] M.H. Hanigan, B.C. Gallagher, P.T. Jr Taylor, M.K. Large, Inhibition of γ-glutamyl transpeptidase activity by acivicin in vivo protects the kidney from cisplatin-induced toxicity, Cancer Res. 54 (1994) 5925–5929.
[16] M. Tuzova, J.-C. Jean, R. P. Hughey, L. A. Scism Brown, W. Cruikshank, J. Hiratake, M. Joyce-Brady. Inhibiting lung lining fluid glutathione metabolism with GGsTop as a novel treatment for asthma. Front. Pharmacol. http://dx.doi.org/10.3389/fphar.2014.00179S.
[17] M. Ferretti, T. Destro, S.C. Tosatto, et al., γ-Glutamyl transferase in the cell wall participates in extracellular glutathione salvage from the root apoplast, New Phytol. 181 (2009) 115–126.
[18] I. Castellano, A. Merlino, M. Rossi, et al., Biochemical and structural properties of γ-glutamyl transpeptidase from *Geobacillus thermodenitrificans*: an enzyme specialized in hydrolase activity, Biochimie 92 (2010) 464–474.
[19] I. Castellano, A. Di Salle, A. Merlino, et al., Gene cloning and protein expression of γ-glutamyltranspeptidases from *Thermus thermophilus* and *Deinococcus radiodurans*: comparison of molecular and structural properties with mesophilic counterparts, Extremophiles 15 (2011) 259–270.
[20] H. Suzuki, C. Yamada, K. Kato, Amino Acids 32 (2007) 333–340.
[21] H. Suzuki, C. Miwa, S. Ishihara, et al., A single amino acid substitution converts γ-glutamyltranspeptidase to a class IV cephalosporin acylase (glutaryl-7-aminocephalosporanic acid acylase), Appl. Environ. Microbiol. 70 (2004) 6324–6328.
[22] H. Minami, H. Suzuki, H. Kumagai, A mutant *Bacillus subtilis* γ-glutamyl transpeptidase specialized in hydrolysis activity, FEMS Microbiol. Lett. 224 (2) (2003) 126–130.
[23] H. Suzuki, S. Izuka, N. Miyakawa, et al., Enzymatic production of theanine, an 'umami' component of tea, from glutamine and ethylamine with bacterial γ-glutamyltranspeptidase, Enzyme Microb. Technol. 31 (2002) 884–889.
[24] H. Zhang, Y. Zhan, J. Chang, J. Liu, L. Xu, Z. Wang, Q. Liu, Q. Liao, Enzymatic synthesis β-N-(γ-L(+)-glutamyl)phenylhydrazine with *Escherichia coli* γ-glutamyltranspeptidase, Biotechnol. Lett. 34 (2012) 1931–1935.
[25] T. Okada, H. Suzuki, K. Wada, et al., Crystal structures of γ-glutamyltranspeptidase from *Escherichia coli*, a key enzyme in glutathione metabolism, and its reaction intermediate, Proc. Natl. Acad. Sci. U. S. A. 103 (2006) 6471–6476.
[26] T. Okada, H. Suzuki, K. Wada, et al., Crystal structure of the γ-glutamyltranspeptidase precursor protein from *Escherichia coli*. Structural changes upon autocatalytic processing and implications for the maturation mechanism, J. Biol. Chem. 282 (2007) 2433–2439.
[27] G. Boanca, A. Sand, J.J. Barycki, Uncoupling the enzymatic and autoprocessing activities of *Helicobacter pylori* γ-glutamyltranspeptidase, J. Biol. Chem. 281 (2006) 19029–19037.
[28] Boanca, A. Sand, T. Okada, et al., Autoprocessing of *Helicobacter pylori* γ-glutamyltranspeptidase leads to the formation of a threonine–threonine catalytic dyad, J. Biol. Chem. 282 (2007) 534–541.
[29] A. Pica, I. Russo Krauss, I. Castellano, et al., Exploring the unfolding mechanism of γ-glutamyltranspeptidases: the case of the thermophilic enzyme from *Geobacillus thermodenitrificans*, Biochim. Biophys. Acta-Proteins Proteomics 1824 (2012) 571–577.
[30] A. Pica, I. Russo Krauss, I. Castellano, et al., Effect of NaCl on the conformational stability of the thermophilic γ-glutamyltranspeptidase from *Geobacillus thermodenitrificans*: implication for globular protein halotolerance, Biochim. Biophys. Acta Proteins Proteomics 1834 (2013) 149–157.
[31] M.B. West, M.H. Hanigan, γ-Glutamyl transpeptidase is a heavily N-glycosylated heterodimer in HepG2 cells, Arch. Biochem. Biophys. 504 (2) (2010) 177–181.
[32] M.B. West, S. Wickham, L.M. Quinalty, R.E. Pavlovicz, C. Li, M.H. Hanigan, Autocatalytic cleavage of human γ-glutamyl transpeptidase is highly dependent on N-glycosylation at asparagine 95, J. Biol. Chem. 286 (2011) 28876–28888.
[33] M.B. West, Y. Chen, S. Wickham, et al., Novel insights into eukaryotic γ-glutamyltranspeptidase 1 from the crystal structure of the glutamate-bound human enzyme, J. Biol. Chem. 288 (2013) 31902–31913.
[34] K. Wada, M. Irie, H. Suzuki, et al., Crystal structure of the halotolerant γ-glutamyltranspeptidase from *Bacillus subtilis* in complex with glutamate reveals a unique architecture of the solvent-exposed catalytic pocket, FEBS J. 277 (2010) 1000–1009.
[35] L.-L. Lin, P.R. Chou, Y.W. Hua, et al., Overexpression, one-step purification, and biochemical characterization of a recombinant γ-glutamyltranspeptidase from *Bacillus licheniformis*, Appl. Microbiol. Biotechnol. 73 (2006) 103–112.
[36] M.-C. Chi, Y.-Y. Chen, H.-F. Lo, L.-L. Lin, Experimental evidence for the involvement of amino acid residue Glu398 in the autocatalytic processing of *Bacillus licheniformis* γ-glutamyltranspeptidase, Febs Open Biol. 2 (2012) 299–304.
[37] S.S. Tate, A. Meister, Interaction of γ-glutamyl transpeptidase with amino acids, dipeptides, and derivatives and analogs of glutathione, J. Biol. Chem. 249 (1974) 7593–7602.
[38] G. Böhm, R. Muhr, R. Jaenicke, Quantitative analysis of protein far UV circular dichroism spectra by neural networks, Protein Eng. 5 (1992) 191–195.
[39] J.M. Scholtz, G.R. Grimsley, C.N. Pace, Solvent denaturation of proteins and interpretations of the m value, Methods Enzymol. 466 (2009) 549–565.
[40] L.-L. Lin, M.-C. Lin, Y.-Y. Chen, A. Merlino, Low resolution X-ray structure of γ-glutamyltranspeptidase from *Bacillus licheniformis*: opened active site cleft and a cluster of acid residues potentially involved in the recognition of a metal ion, Biochim. Biophys. Acta Proteins Proteomics 1844 (2014) 1523–1529.
[41] N. Guex, M.C. Peitsch, T. Schwede, Automated comparative protein structure modeling with SWISS-MODEL and Swiss-PdbViewer: a historical perspective, Electrophoresis 30 (Suppl. 1) (2009) S162–S173.

[42] W.L. DeLano, New York: Schrödinger, LLC, 2010. The PyMOL Molecular Graphics System, Version 1.3r1, 2010.
[43] D. Kishore, S. Kundu, A.M. Kayastha, Thermal, chemical and pH induced denaturation of a multimeric β-galactosidase reveals multiple unfolding pathways, PLoS One 7 (11) (2012) e50380.
[44] A. Merlino, I. Russo Krauss, I. Castellano, E. De Vendittis, B. Rossi, M. Conte, A. Vergara, F. Sica, Structure and flexibility in cold-adapted iron superoxide dismutases: the case of the enzyme isolated from *Pseudoalteromonas haloplanktis*, J. Struct. Biol. 172 (2010) 343–352.
[45] A. Merlino, I. Russo Krauss, I. Castellano, A. Capasso, M.R. Ruocco, E. De Vendittis, B. Rossi, F. Sica, Structural and denaturation studies of two mutants of a cold adapted superoxide dismutase point to the importance of electrostatic interactions in protein stability, Biochim. Biophys. Acta Proteins Proteomics 1844 (2014) 632–640.
[46] V. Granata, P. Del Vecchio, G. Barone, E. Shehi, P. Fusi, P. Tortora, G. Graziano, Guanidine-induced unfolding of the Sso7d protein from the hyperthermophilic archaeon *Sulfolobus solfataricus*, Int. J. Biol. Macromol. 34 (2004) 195–201.